

# Deep Heterogeneous Autoencoder for Subspace Clustering of Sequential Data

Abubakar Siddique<sup>1</sup>, Reza Jalil Mozhdehi<sup>1</sup>, and Henry Medeiros<sup>1</sup>

Marquette University, Milwaukee WI 53233, USA

{abubakar.siddique,reza.jalilmozhdehi,henry.medeiros}@marquette.edu

**Abstract.** We propose an unsupervised learning approach using a convolutional and fully connected autoencoder, which we call deep heterogeneous autoencoder, to learn discriminative features from segmentation masks and detection bounding boxes. To learn the mask shape information and its corresponding location in an input image, we extract coarse masks from a pretrained semantic segmentation network as well as their corresponding bounding boxes. We train the autoencoders jointly using task-dependent uncertainty weights to generate common latent features. The feature vector is then fed to the k-means clustering algorithm to separate the data points in the latent space. Finally, we incorporate additional penalties in the form of a constraints graph based on prior knowledge of the sequential data to increase clustering robustness. We evaluate the performance of our method using both synthetic and real world multi-object video datasets to demonstrate the applicability of our proposed model. Our results show that the proposed technique outperforms several state-of-the-art methods on challenging video sequences.

## 1 Introduction

Subspace clustering algorithms applied to sequential data can separate sequences of similar data points into disjoint groups. State-of-the-art subspace clustering methods have shown promising performance on single object patches [1], video sequences [2], and face tracking datasets [3]. For multi-object video sequences, subspace clustering is a challenging task since the pose, shape, and appearance of the objects may change with time. In addition, the data distribution over time has significant variations due to misdetections, occlusions, and fast motions. Due to these challenges, subspace clustering in video segments using only location [4,5], shape [6,7,8], or appearance [3,9] features might not produce satisfactory results.

The goal of this work is to use multiple cues from sequential data to increase the discriminative capability of the latent representations. Traditional subspace clustering techniques are trained based only on shape/appearance information [6,10,8] or on location information, generally in the form of bounding boxes [4]. Instead, in this work, we jointly learn a latent feature that encompasses both. As the subspace size increases, the challenges described above are exacerbated, but our approach learns location and shape information jointly using a multi-task

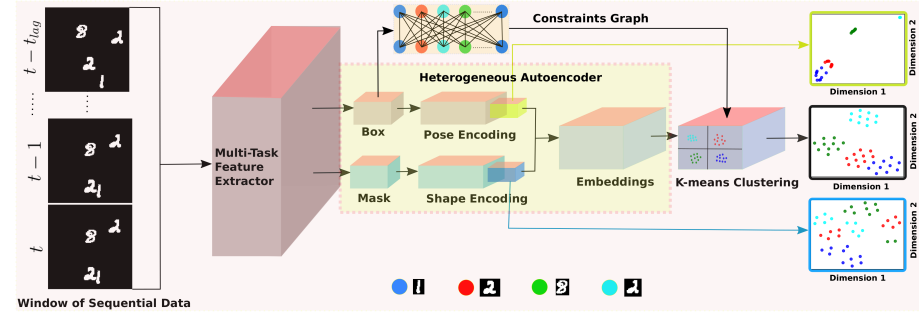


**Fig. 1.** Proposed multi-task learning based subspace clustering framework.

convolutional and fully connected autoencoder, which we call Deep Heterogeneous Autoencoder (DHAE).

In this work, we address the challenges of clustering sequential data segments using multi-task learning [11]. To optimally learn the weights from multiple cues in sequential data, we formulate the multi-task loss function using maximum Gaussian log-likelihoods with task-dependent uncertainties [12]. We propose an unsupervised technique to learn multiple tasks from sequential data optimally so that similar data points become closer and dissimilar points are separated further. In summary, we provide four main contributions:

1. We propose a novel unsupervised approach to learn shape and location features jointly with multi-task weighting, which solves the subspace clustering challenges in sequential data.
2. We propose a new data partitioning algorithm based on constrained k-means to incorporate prior knowledge of the sequential data, which reduces matching failures.
3. We evaluate our model on two synthetic and three real world datasets. To make the synthetic data realistic, we consider most of the challenges commonly observed in videos, such as pose, shape, and appearance variations. In our ablation study, we discuss the importance of each component of our model.
4. Upon acceptance of this submission, the source code will be made publicly available.

## 2 Related Work

Subspace clustering is an unsupervised learning problem in which data points are mapped to one or more lower dimensionality subspaces where it is easier to make inferences about the relationships among different data points. Many clustering methods have been developed for both linear and non-linear subspaces.

These methods employ two common strategies: i) extract low-dimensional discriminative features, ii) apply a robust clustering approach to partition the subspaces. Earlier state-of-the-art approaches employed methods based on factorization strategies [1,13] or kernels [14,15,16,17] to separate the data points into their respective subspaces. For example, sparse subspace clustering (SSC) [1] learns an affinity matrix where non-zero entries correspond to the data points from the same subspace and there is no intersection between subspaces. The lowest rank representation (LRR) [18] also incorporates the global structure of the data points by using a rank penalty.

More recent methods employ convolutional neural networks [7,6,9], or generative adversarial networks [19,8] oftentimes in conjunction with self-expressive layers [6,8]. The autoencoder-based deep subspace clustering network (DSC-Net) [6] uses fully connected layers to learn an affinity matrix that enhances the discriminative property of the embeddings for non-linear subspaces. Some autoencoder-based techniques consider both the subspace reconstruction error and the clustering error for better sample distribution [20]. However, few methods [3,2,21] address the challenges of sequential data, which must take into account the fact that object features may change abruptly over time [22,23,24]. Although existing subspace clustering approaches may be able to find discriminative features to cluster static data, these features may not be sufficiently distinctive to identify the subspaces corresponding to multiple objects in sequential data. Subspace clustering in multi-object sequential data is an under-explored problem, particularly in real world applications.

Clustering in sequential data is challenging due to pose, shape, and appearance variations. The ordered subspace clustering (OSC) algorithm [21] considers sequential data, but it mostly learns to cluster single object sequences as a single task. Instead, we employ multi-task learning [25,12] using our proposed DHAЕ to generate more effective latent representations of sequential multi-object data. We also use prior knowledge regarding the sequential data in the form of a constraints graph [26] to improve clustering robustness. Thus, our unsupervised learning approach does not require explicit cluster assignment learning [7].

### 3 Subspace Clustering for Sequential Data

As Fig. 1 illustrates, our spatio-temporal subspace clustering framework extracts features of interest from the objects in each video frame using a multi-task feature extractor module. We then use our proposed DHAЕ to generate a discriminative latent representation of the pose and shape of each object based on these input features. To establish the temporal coherence among targets, we adopt a graph method [27] in the temporal window to preclude the association of points that violate a set of constraints that are known to hold in the scenario under consideration. For example, no two detections are allowed to belong to the same cluster if their timestamps are identical. Finally, we use the constrained k-means algorithm [26] to estimate the correct label of the targets by minimizing

the dissimilarity of their latent representations while satisfying the association constraints. We describe each component of our method in more detail below.

### 3.1 Multi-Task Feature Extractor

The multi-task feature extractor (MTFE) module is responsible for generating the segmentation masks and bounding boxes of the objects of interest in each video frame. This task is independent of the proposed temporal clustering mechanism and can be performed by any supervised or unsupervised image segmentation method such as [28,29]. More specifically, let  $x_{b,o}^t \in \mathbb{R}^N$  be the detected bounding box of the  $o$ -th target observed at time  $t$  and let  $x_{m,b}^t \in \mathbb{R}^{M \times M}$  be a binary segmentation mask representing the shape of that object. The MTFE takes as input a video frame  $I^t$  and generates the set

$$\mathcal{X}^t = \{[x_{m,o}^t, x_{b,o}^t]\}_{o=1}^{\mathcal{O}^t}, \quad (1)$$

where  $\mathcal{O}^t$  is the number of unique objects at time  $t$ .

As explained in detail in Section 3.2, we use the shape and location features (i.e., the segmentation masks and the bounding boxes) generated by MTFE to learn a latent representation using a multi-task framework with task-dependent uncertainties, as described in [25,12].

### 3.2 Deep Heterogeneous Autoencoder

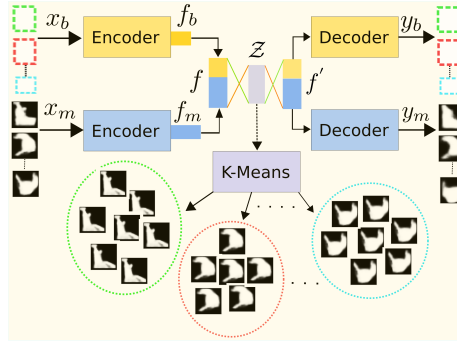
Clustering methods that resort only to object appearance information do not perform well when multiple objects are observed simultaneously in a sequence of video frames. As the number of objects of interest of a certain category (e.g., pedestrians) observed in a given frame increases, the average appearance differences among the objects becomes increasingly lower. At the same time, as the duration of the temporal segment in which the objects are observed increases, the variability in the appearance of any given target becomes increasingly higher. Hence, to allow for sufficient temporal appearance variability while preventing incorrect associations among temporally proximal observations, we incorporate location information into the latent feature representation. In other words, to address the problem of clustering multiple objects in videos, we propose to learn shape and location information jointly.

Fig. 2 shows our proposed DHAE architecture. To combine the coarse mask and location information, we design a network consisting of three parts: i) a pair of encoders that take as input the  $N$ -dimensional location vector  $x_b^1$  and the  $M \times M$  mask  $x_m$ , ii) an uncertainty-aware module based on self-expressive layers [6] to reconstruct the concatenated feature  $f'$  and learn the latent feature  $\mathcal{Z}$ , iii) a pair of decoders to reconstruct the bounding box  $y_b$  and the mask  $y_m$ . The DHAE takes the extracted set of shapes and locations from the MTFE and

---

<sup>1</sup> To simplify the notation, we drop the subscript  $o$  and the superscript  $t$ .

reconstructs them by minimizing the combined reconstruction loss. To incorporate the location features  $x_b$  into our model, we employ a fully connected auto-encoder (AE) with  $N$  inputs, which is represented by the yellow boxes in Fig. 2. The corresponding encoded feature vector is  $f_b = h_b(x_b)$ , where  $h_b : \mathbb{R}^N \rightarrow \mathbb{R}^F$  is the encoding function. The shape information  $x_m$  is encoded by a convolutional auto-encoder (CAE) with an input size of  $M \times M$ , which is represented by the blue boxes in Fig. 2. Let  $f_m = h_m(x_m)$  be the latent feature of the CAE, where  $h_m : \mathbb{R}^{M \times M} \rightarrow \mathbb{R}^F$  is the encoding function. A function  $h_a : \mathbb{R}^{2F} \rightarrow \mathbb{R}^{2F}$  takes the concatenated feature vector  $f = [f_m, f_b]$  and converts it into the latent representation  $\mathcal{Z} \in \mathbb{R}^{2F}$ . A function  $h'_a : \mathbb{R}^{2F} \rightarrow \mathbb{R}^{2F}$  then takes the latent representation  $\mathcal{Z}$  and produces a new feature  $f' = [f'_m, f'_b]$ , which combines both shape and location information. We then process the two components of the feature vector separately using the decoders of the two autoencoders. That is, the output produced by the decoding function  $h'_m : \mathbb{R}^F \rightarrow \mathbb{R}^{M \times M}$  is  $y_m \in \mathbb{R}^{M \times M}$  and the decoding function  $h'_b : \mathbb{R}^F \rightarrow \mathbb{R}^N$  produces  $y_b \in \mathbb{R}^N$ .



**Fig. 2.** Proposed DHAE model architecture which jointly learns shape and location information for subspace clustering in sequential data.

We integrate the CAE and the AE into a single network and train it using the reconstruction errors for  $y_m$  and  $y_b$  simultaneously using the following multi-task cost function

$$\mathcal{L} = \alpha l_m(x_m, y_m) + \beta l_b(x_b, y_b), \quad (2)$$

where  $l_m(\cdot)$  and  $l_b(\cdot)$  are the mean squared error losses corresponding to the shape and location errors respectively, and  $0 \leq \alpha, \beta \leq 1$  are the weights that determine their relative contributions to the error. As explained in the next section, these weights are determined using a multi-task likelihood model.

**Multi-task Likelihood** We formulate the multi-task loss function using maximum Gaussian log-likelihoods with task-dependent uncertainties [25,12]. Let  $f^W(x) = [f_m^W(x), f_b^W(x)]$  be the output of the proposed DHAE with weights  $W$ ,

input vector  $x = [x_m, x_b]$ , and predicted output  $y = [y_m, y_b]$ . The likelihood for the regression task can be defined as

$$p(y_m, y_b | f^W(x)) = p(y_m | f_m^W(x)) \cdot p(y_b | f_b^W(x)). \quad (3)$$

Thus, the cost function,  $\mathcal{L}(W, \sigma_m, \sigma_b)$  for our DHAE model is given by

$$\begin{aligned} \mathcal{L}(W, \sigma_m, \sigma_b) &= -\log p(y_m, y_b | f^W(x)) \\ &\propto \frac{1}{2\sigma_m^2} \|y_m - f_m^W(x)\|^2 + \frac{1}{2\sigma_b^2} \|y_b - f_b^W(x)\|^2 + \log \sigma_m \sigma_b \\ &= \frac{1}{2\sigma_m^2} l_m(x_m, y_m) + \frac{1}{2\sigma_b^2} l_b(x_b, y_b) + \log \sigma_m \sigma_b, \end{aligned} \quad (4)$$

where  $\sigma_m$  and  $\sigma_b$  are the model noise parameters. For noisy outputs, if  $\sigma_m$  or  $\sigma_b$  is large, the corresponding contribution of  $l_m(\cdot)$  or  $l_b(\cdot)$  will decrease accordingly. The last term of the objective function acts as a regularizer, preventing the noise from increasing too much. Thus, we learn the relative weights of each loss function term based on the uncertainty of the training data.

**Network Implementation and Training Details** Our AE has an input size of  $N = 4$  and one fully connected layer of size 64. Our CAE uses 5 convolutional layers with kernel size  $3 \times 3$ , ReLU activations, and a stride of  $2 \times 2$  for down-sampling and upsampling [30]. The size of the input layer is  $M = 128$  and the subsequent layers have half the size of the previous layer. The number of convolutional channels in each layer is 16, 16, 32, 32, and 48 (the decoder mirrors the structure of the encoder). For lower resolution test sequences (MNIST, Sprite),  $M = 28$ , and the number of convolutional channels in each layer is 16, 8, 8, 8, 4. The functions  $h_a(\cdot)$  and  $h'_a(\cdot)$  in the self-expressive layer are implemented using fully connected layers of size  $F = 64$ . We train the network using stochastic gradient descent with ADADELTA [31] learning rate adaptation.

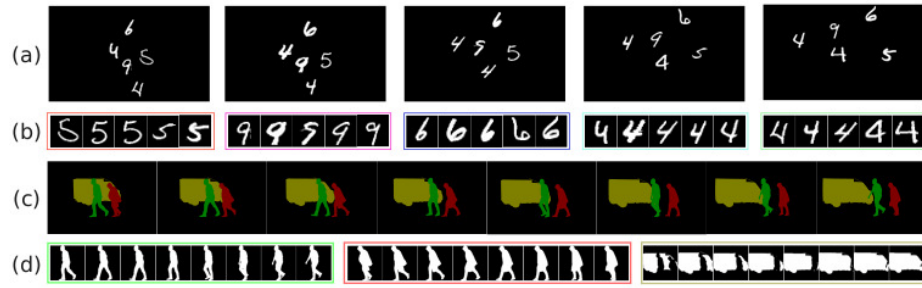


**Fig. 3.** Subspace examples for (a) MNIST-MOT and (c) DAVIS sequence. (a) and (c) show the frames in a temporal window. (b) and (d) show the corresponding subspaces.

### 3.3 Spatio-temporal Clustering

To overcome the challenges of abrupt scale, shape, and pose variations in multiple-object video sequences, we cluster the objects over a temporal window comprising the  $t_{lag}$  frames preceding the current frame at time  $t$  (Fig. 3). That is, at each time instant  $t$ , we generate a corresponding temporal sliding window  $\mathcal{T}^t = \{t - t_{lag}, t - t_{lag+1}, \dots, t\}$ . Since the window is computed at each frame, there is an overlap of  $t_{lag} - 1$  frames between the windows at time  $t$  and  $t + 1$ . Hence, the corresponding data points used to form the subspace cluster in each window of a video sequence are shared. The input to our spatio-temporal subspace clustering algorithm (Alg. 1) is the set of frames  $\{I^t\}_{t=1}^T$  where  $T$  is the number of frames in the video. Our algorithm iterates over the temporal windows  $\mathcal{T}^t$  for  $t = 1, 2, \dots, T$  to construct the sets  $\mathcal{W}^t = \{\mathcal{X}^{t'} | t' \in \mathcal{T}^t\}$ , where  $\mathcal{X}^{t'}$  is the output of the MTFE for frame  $I^{t'}$ . The algorithm then clusters the detections within each window using the embedded representations  $\mathcal{Z}^t = \{z_o^{t'} | t' \in \mathcal{T}^t, o \in \{1, \dots, \mathcal{O}^{t'}\}\}$  generated by the DHAE and the constrained k-means algorithm. The formulation of the constraint graph  $\mathcal{G}^t$  and the constrained k-means algorithm are described in Section 3.4.

---

**Algorithm 1** Subspace clustering algorithm

---

**Input:** Set of video frames  $\{I^t\}_{t=1}^T$   
**Output:** Subspace clusters  $\mathcal{C}_K$

- 1: **repeat**
- 2:      $\mathcal{W}^t = \text{MTFE}(\{I^{t'} | t' \in \mathcal{T}^t\})$
- 3:      $\mathcal{Z}^t = \text{DHAE}(\mathcal{W}^t)$
- 4:     Compute  $\mathcal{G}^t$  using Eqs. (5)-(7)
- 5:      $\mathcal{C}_K = \emptyset$
- 6:      $\mathcal{C}_t = \text{k-means}(\mathcal{Z}_t, \mathcal{G}^t)$
- 7:     **for**  $Q \in \mathcal{C}_t$  **do**
- 8:          $\bar{\tau} = \frac{\sum_{d_i \in Q} \text{score}(d_i)}{|Q|}$
- 9:         **if**  $\bar{\tau} > \lambda$  **then**
- 10:              $\mathcal{C}_K = \mathcal{C}_K \cup \{Q\}$
- 11:         **end if**
- 12:     **end for**
- 13: **until** end of the video sequence

---

Each call to the **k-means**( $\cdot$ ) algorithm (line 6 in Alg. 1) produces a set of clusters  $\mathcal{C}_t$  whose elements are sets of detections that have been assigned to the same object (Section 3.4 discusses our approach to determine the number of clusters at each window). For each cluster, the predicted cluster labels are then used to compute the total cluster probability. To remove false positive detections, we then select only the clusters with high total probability score. The normalized probability score  $\bar{\tau}$  of cluster  $Q \in \mathcal{C}_t$ , which is defined as the ratio between  $\sum_{d_i \in Q} \text{score}(d_i)$  (total score of cluster  $Q$ ) and  $|Q|$ , is computed

in line 8. The procedure  $\text{score}(d_i)$  returns the confidence score of detection  $d_i$ . Line 9 of Alg. 1 discards clusters with scores lower than a threshold  $\lambda$ . Clusters that satisfy the score threshold are included in the resulting cluster set  $\mathcal{C}_K$ .

### 3.4 Sequential Data Constraints

In spatio-temporal subspace clustering, constraints based on prior knowledge regarding the sequential data may reduce association mistakes by imposing penalties on unlikely pairwise matching. We use an undirected graph  $\mathcal{G}^t$  to encode the constraints among pairs of detections in the temporal window  $\mathcal{T}^t$ . This graph determines which pairs of detections cannot belong to the same cluster based on their known temporal and spatial relationships. The constrained k-means algorithm [26] then minimizes the Euclidean distances between the cluster centroids and mutually compatible detections while precluding pairs of detections in  $\mathcal{G}^t$  to be assigned to the same cluster. These constraints reduce the failures caused by similarities in the time and space domains even though the pair of instances belongs to a different object.

**Constraints Graph Formulation** To incorporate prior knowledge regarding object correspondences in the temporal sliding windows, we construct the *cannot link graph*  $\mathcal{G}^t = (V^t, E^t)$ . The vertices of the graph correspond to the set of bounding boxes in all the frames in the window  $\mathcal{T}^t$ , i.e.,

$$V^t = \{x_{b,o}^t \mid t \in \mathcal{T}^t, o \in \{1, \dots, \mathcal{O}^t\}\}. \quad (5)$$

The set of edges consists of pairs of nodes  $v_m$  and  $v_n$  that do not meet the spatial and temporal restrictions imposed by the *cannot link function*  $f_{cl}(\cdot)$ , i.e.,

$$E^t = \{(v_m, v_n) \mid v_m \in V^t, v_n \in V^t, f_{cl}(v_m, v_n) = 1\}. \quad (6)$$

The *cannot link function* restricts the association between vertices from the same frame and from vertices in close temporal proximity that do not overlap, i.e.,

$$f_{cl}(v_m, v_n) = \begin{cases} 1 & \text{if } t_m = t_n \\ 1 & \text{if } \text{iou}(v_m, v_n) = 0, \quad t_m - t_n \leq \tau, \\ 0 & \text{otherwise} \end{cases} \quad (7)$$

where  $t_m$  and  $t_n$  are the timestamps for the detections corresponding to nodes  $v_m$  and  $v_n$ , and the function  $\text{iou}(\cdot)$  computes their intersection over union.

**Constrained K-means** In the constrained k-means algorithm [26], a node  $v_m$  may be assigned to the same cluster as  $v_n$  only if the edge  $(v_m, v_n) \notin E^t$ . We cluster objects that do not satisfy the *cannot link* constraints by minimizing the distance between their corresponding latent features  $z_o^t$  and the cluster centroids  $z_k \in \mathcal{K}$ , where  $\mathcal{K}$  is the set of cluster centroids, which are initialized using the

k-means++ algorithm [32]. The objective of our algorithm is to associate each embedded feature  $z_o^t \in \mathcal{Z}^t$  to a unique cluster with centroid  $z_k$  while minimizing the cost

$$L(\mathcal{K}) = \sum_{z_k \in \mathcal{K}} \sum_{z_o^t \in \mathcal{Z}^t} \|z_k - z_o^t\|^2. \quad (8)$$

Thus, our approach groups the nodes into  $|\mathcal{K}|$  disjoint clusters  $C_1, \dots, C_{|\mathcal{K}|}$  while assuring that two feature vectors  $z_m, z_n$  can only belong to the same cluster  $C_i$  if the corresponding edge  $(v_m, v_n) \notin E^t$ . That is, the nodes are grouped into subsets which contain only nodes from distinct frames and such that their corresponding bounding boxes have an intersection over union greater than zero when the temporal difference between them is less than  $\tau$ .

The dimensionality of the subspace corresponding to the window  $\mathcal{T}^t$  is given by the total number of objects observed during that period. Hence, it is an unknown parameter. Although designing a robust mechanism to determine the number of clusters  $|\mathcal{K}|$  is a challenging task, which is beyond the scope of this work, we employ a simple strategy to determine its approximate value. Our approach consists of setting the number of clusters to the maximum number of targets observed in a single frame within the window  $\mathcal{T}^t$ , i.e.,

$$|\mathcal{K}| = \max_{t' \in \mathcal{T}^t} \mathcal{O}^{t'}. \quad (9)$$

**Table 1.** Specifications of the evaluation dataset.

Dataset	#Seq.	#Obj.	Instances	Shape	Challenge: randomly changed cues
MNIST-MOT	20	1061	51545	$28 \times 28$	pose, shape, motion
MNIST-MOT*	20	883	42906	$28 \times 28$	birth/death, pose, scale, shape, motion
Sprites-MOT	20	1782	85890	$28 \times 28$	birth/death, pose, scale, shape, motion
DAVIS	90	207	13561	$128 \times 128$	scale, shape, object categories
MOTS-KITTI	9	210	10738	$128 \times 128$	birth/death, pose, scale, shape, motion, moving camera, crowded
MOTS-MOT17	4	228	26890	$128 \times 128$	cues in MOTS-KITTI

## 4 Datasets and Experiments

We evaluate the performance of subspace clustering in sequential data using our proposed DHAЕ on two synthetic and two real world datasets. The synthetic datasets are: i) MNIST-MOT [33] and ii) Sprites-MOT [33]. The reasons for using synthetic datasets are: i) it is easy to control the difficulties in MOT scenarios such as abrupt pose, scale, and shape variations, ii) the bounding box and segmentation mask annotations for multiple objects in crowded scenarios are readily available. Then we employ the recently published Multi-Object Tracking and Segmentation (MOTS) [34] benchmark and DAVIS [35] datasets to investigate how well our model can cluster multiple objects in real world videos. Table 1 summarizes the characteristics of the datasets we used in our evaluation.

#### 4.1 Synthetic Data

We generate synthetic MNIST-MOT and Sprites-MOT sequences using the procedure described in [33], which includes most of the common challenges observed in MOT problems, such as high object density, objects entering and leaving the scene, as well as velocity, shape, and pose variations. For the MNIST-MOT dataset, we generate 9 digit classes and for Sprites-MOT we generate 4 geometric shapes. For both datasets, the object density is  $3 \leq |O| \leq 5$ , and the size of the objects is  $28 \times 28$  at each frame of size  $256 \times 256$ . We generate 20 video sequences with 500 frames for each dataset. In each sequence, the set of initial objects (digits or sprites) is chosen randomly at the first frame. In the subsequent frames, the objects move in random directions. To include the challenges of real world videos, we change the shapes at an interval of 5 frames by randomly selecting a different instance of the corresponding object. To assess the impact of variable cluster sizes, we create two versions of the MNIST-MOT dataset. While the MNIST-MOT dataset has a fixed number of objects, the MNIST-MOT\* dataset allows objects to enter and leave the scene. To train our proposed DHAE, we extract the bounding box and shape mask of each object from the synthetic video frames using separate training sequences.

#### 4.2 MOTS Dataset

The MOTS benchmark dataset consists of the MOT17 [36] and KITTI [37] video sequences where multiple objects (vehicles and pedestrians) are annotated with their segmentation masks. The MOTS-MOT17 dataset consists of four fully annotated videos of crowded scenes and the MOTS-KITTI dataset consists of 21 videos acquired from a moving car. Both datasets contain objects with abrupt scale and shape variations across time. In our evaluation, we use the instance segmentation masks and bounding boxes from the ground truth as well as detections generated by an instance segmentation network [28]. We use the annotated video datasets for clustering evaluation because the metrics require a known number of clusters  $k$  in a video segment. For clustering multiple objects in a real video, the value of  $k$  is unknown and we also address this challenge using Eq. 9. To train our DHAE, we use extracted features from 12 MOTS-KITTI sequences. We used the remaining sequences for testing (Table 1).

#### 4.3 DAVIS Dataset

Generating annotated videos with bounding boxes and segmentation masks is a notoriously challenging task. To further demonstrate the effectiveness of our algorithm, we also employ the publicly available DAVIS video object segmentation dataset [35] even though the sequences are less crowded than in the MOTS datasets. For the DAVIS dataset, we extract bounding boxes and segmentation masks from the annotated videos to test our clustering algorithm. We use DAVIS dataset only for performance evaluation.

**Table 2.** Comparison of clustering performance on *MNIST-MOT* ( $t_{lag} = 5$ ,  $k = |O| = 3$ ) and *MNIST-MOT\** sequences ( $t_{lag} = 5$ ,  $|O| = 5$ ,  $k$  (Eq. 9) varies in a range,  $1 \dots |O|$ ).

Configuration	MNIST-MOT				MNIST-MOT*			
	ACC	PUR	NMI	ARI	ACC	PUR	NMI	ARI
DEC [7]	0.87	0.89	0.88	0.81	0.84	0.85	0.89	0.78
ClusterGAN [19]	0.81	0.78	0.82	0.80	0.71	0.75	0.58	0.80
Shape Embed	0.90	0.90	0.82	0.75	0.85	0.87	0.84	0.72
Loc Embed	0.96	0.95	0.94	0.91	0.91	0.92	0.92	0.85
Loc+Shape	<b>0.97</b>	<b>0.96</b>	<b>0.95</b>	<b>0.92</b>	<b>0.92</b>	<b>0.93</b>	<b>0.93</b>	<b>0.86</b>
<b>Loc+Shape+<math>\mathcal{G}^t</math></b>	<b>0.99</b>	<b>0.99</b>	<b>0.99</b>	<b>0.98</b>	<b>0.96</b>	<b>0.97</b>	<b>0.97</b>	<b>0.95</b>

## 5 Results and Discussions

### 5.1 Evaluation Metrics

To evaluate our proposed approach, we adopt the popular clustering performance assessment metrics: accuracy (ACC), purity (PUR), normalized mutual information (NMI) [8,38], and adjusted random index (ARI) [39] for noise free detections (annotated videos). However, for the clustering performance in real videos we employ the multi-object detection (MOD) [40] metrics.

### 5.2 Digit Clustering

We evaluate the proposed approach on the MNIST-MOT dataset for clustering the multiple moving digits in the temporal segments. We apply the extracted cues to DHAE for clustering them in the jointly learned latent space using constrained k-means. Since we update the temporal segment at each  $t$  with stride 1, the final evaluated clustering metrics are the average over all the possible segments in the entire dataset. Table 2 summarizes the clustering results for different multi-object challenges on MNIST-MOT according to the evaluation procedure described in [19,8]. Although the location features play a critical role in clustering multiple moving targets, shape features also contribute significantly to the performance of our approach. As the t-SNE visualization in Fig. 1 illustrates, as the digits 2 and 1 approach each other, their corresponding embeddings remain separable. In Table 2, the shape-only model performs worse in comparison with location since both versions of the MNIST dataset periodically change the target shape, which reduces the benefits of shape features (Table 3 shows that the benefits of shape features in real videos are more pronounced). Due to the lack of availability of methods that perform clustering based on location and shape features, we select two state-of-the-art clustering methods for performance comparison [19,7]. Although those baselines show comparable performance with our model when only shape features are used (maximum 9% improvement in terms of ACC), Table 2 shows how the different components of our method increase clustering robustness. More concretely, our joint DHAE model (Loc+Shape) improves over the baselines by 10% and 7%, 7% and 11%, 16% and 18%, 13% and

12% in terms of ACC, PUR, NMI, and ARI (*MNIST-MOT* results in Table 2). If we increase the object density and incorporate other multi-object challenges observed in real surveillance videos, our method also shows improvements in terms of most metrics (*MNIST-MOT\** results in Table 2). Moreover, our jointly learned embeddings with achieve much better results than the baseline when we use  $\mathcal{G}^t$ . By using constraints we obtain nearly perfect results with only 1% wrong assignments.

### 5.3 Synthetic Object Clustering

We also evaluate the clustering performance on the Sprites-MOT sequential data [33] where randomly selected objects ( $|O| = 5$ ) move in random directions while showing most of the multi-object video challenges. Table 4 shows that we obtain highly satisfactory clustering metrics ( $ACC > 90\%$ ) when all the components of the DHAЕ-based spatio-temporal clustering technique are employed.

### 5.4 Clustering in Real Videos

Although previous works [21] have employed subspace clustering for video scene segmentation, to the best of our knowledge, this is the first work to propose clustering of multiple moving objects in the segments of a video scene. To experiment with clustering performance in challenging real world video benchmarks, we use the MOTS and DAVIS datasets. The shape and location features from the datasets’ ground truth annotations (as a noise free detections) are embedded by DHAЕ and then partitioned into subspaces using Alg. 1. Table 4 shows that our method clusters the subspaces in the video segments with more than 90% accuracy for all the datasets when all the components of our approach are utilized. The results in the MOTS-KITTI benchmark are 5% – 10% less accurate in terms of NMI and ARI due to the high density of moving objects and to the camera motion. To evaluate the performance of our proposed clustering algorithm using real noisy detections generated by a prediction network [28], we compute the MOD evaluation metrics [36,40] on MOTS-MOT17 video sequences. We employ the MOD evaluation because the presence of misdetections and false positives makes it impossible to apply traditional clustering evaluation metrics. To compare the performance of our approach with that of state-of-the-art techniques, we train the DEC and ClusterGAN models using subsets of the MOTS and DAVIS datasets comprising the segmentation masks of 163 different targets. In our evaluation, we cluster the multi-task embedded features from the DHAЕ and retain only the clusters that satisfy the minimum cluster score  $\lambda$ . Again, we estimate the number of clusters  $k$  using Eq. 9. For a fair comparison, we use the same values of  $\lambda = 0.62$ ,  $t_{lag} = 5$ , and minimum IoU = 0.4 for all the models under consideration. As shown in Table 3, our shape-only model outperforms both state-of-the-art methods for videos 02 and 11 by a significant margin in most of the metrics and show competitive results for videos 05 and 09. The spatio-temporal relation in a video segment is an important cue to further

improve clustering performance. This becomes clear when we observe the substantial performance improvement for our approach over the shape-only model.

**Table 3.** Multi-Object Detection (MOD) evaluation on MOTS-MOT17 using predictions generated by a real world detection algorithm [28].

Video	Model	$\uparrow$ F1	$\uparrow$ Rcll	$\uparrow$ Prcn	$\uparrow$ TP	$\downarrow$ FP	$\downarrow$ FN	$\uparrow$ MODA	$\uparrow$ MODP
02	DEC	64.6	53.2	82.4	3876	830	3412	41.8	76.6
	ClusterGAN	62.5	51.4	79.8	3746	948	3542	38.4	76.3
	<b>Ours-shape</b>	<b>67.0</b>	<b>56.3</b>	<b>82.7</b>	<b>4101</b>	858	<b>3187</b>	<b>44.5</b>	76.0
	<b>Ours-full</b>	<b>77.3</b>	<b>70.1</b>	<b>86.2</b>	<b>5107</b>	<b>815</b>	<b>2181</b>	<b>58.9</b>	<b>76.9</b>
05	DEC	71.7	69.9	73.6	2564	922	1103	44.8	73.4
	ClusterGAN	66.8	63.9	70.0	2343	1006	1324	36.5	73.0
	<b>Ours-shape</b>	70.4	68.1	73.0	2497	925	1170	43.0	<b>74.1</b>
	<b>Ours-full</b>	<b>80.6</b>	<b>81.9</b>	<b>79.3</b>	<b>3005</b>	<b>784</b>	<b>662</b>	<b>60.6</b>	<b>74.3</b>
09	DEC	79.2	76.0	82.7	2398	500	756	60.2	81.7
	ClusterGAN	72.8	66.9	79.8	2110	534	1044	50.0	81.2
	<b>Ours-shape</b>	79.0	<b>76.1</b>	82.1	<b>2401</b>	522	<b>753</b>	59.6	81.3
	<b>Ours-full</b>	<b>89.0</b>	<b>90.8</b>	<b>87.3</b>	<b>2864</b>	<b>418</b>	<b>290</b>	<b>77.6</b>	<b>81.8</b>
11	DEC	74.7	72.3	77.1	4439	1316	1698	50.9	83.7
	ClusterGAN	71.6	68.7	74.8	4216	1421	1921	45.5	83.2
	<b>Ours-shape</b>	<b>76.0</b>	<b>74.0</b>	<b>78.2</b>	<b>4539</b>	<b>1266</b>	<b>1598</b>	<b>53.3</b>	83.6
	<b>Ours-full</b>	<b>81.3</b>	<b>83.7</b>	<b>79.1</b>	<b>5135</b>	<b>1356</b>	<b>1002</b>	<b>61.6</b>	83.7

## 5.5 Ablation Study

In this section, we analyze the impact of each individual component of our model. Table 2 demonstrates that using the joint location and shape embeddings improves the performance over employing embeddings based either only on location or shape. It should be noted that either embedding alone still shows competitive performance with respect to the state-of-the-art approaches. Finally, the table also demonstrates that the constraint graph further improves clustering performance.

Table 4 shows the impact of the constraint graph  $\mathcal{G}^t$ , of the uncertainty-aware multitask learning loss of Eq. 4, and of using the number of clusters  $k$  as a prior versus estimating it using Eq. 9. As the table indicates, the constraint graph leads to consistent improvements in all the metrics. We also observe the positive impact of multi-task learning using task uncertainties instead of weighting the tasks arbitrarily ( $\alpha = \beta = 0.5$  in Eq. 2). Finally, since in real world videos the number of subspaces is an unknown parameter, estimating  $k$  from the video segments using Eq. 9 leads to a small performance degradation of at most 0.05 (ARI in the DAVIS dataset) when the additional components of our method are used. In summary, Table 4 shows an improvement of the ACC metric of 17%,

**Table 4.** Ablation study for different components of our method. Here, we experiment the clustering performance on unknown number of subspaces  $k$ , constraints graph  $\mathcal{G}^t$ , and multi-task learning (MTL) in DHAE ( $t_{lag} = 10$ ).

Data.	$\mathcal{G}^t$	MTL	Prior $k$	ACC	PUR	NMI	ARI
Sprites-MOT	✗	✗	✗	0.74	0.77	0.75	0.59
	✗	✓	✗	0.77	0.73	0.77	0.60
	✗	✓	✓	0.88	0.90	0.90	0.80
	✓	✓	✗	<b>0.90</b>	<b>0.93</b>	<b>0.91</b>	<b>0.86</b>
	✓	✓	✓	<b>0.91</b>	<b>0.93</b>	<b>0.91</b>	<b>0.86</b>
DAVIS	✗	✗	✗	0.94	0.94	0.95	0.90
	✗	✓	✗	0.95	0.95	0.95	0.90
	✗	✓	✓	0.97	0.97	0.96	0.95
	✓	✓	✗	0.95	0.95	0.95	0.90
	✓	✓	✓	<b>0.98</b>	<b>0.98</b>	<b>0.97</b>	<b>0.95</b>
MOTS-MOT17	✗	✗	✗	0.89	0.91	0.94	0.90
	✗	✓	✗	0.89	0.91	0.94	0.91
	✗	✓	✓	0.90	0.92	0.94	0.91
	✓	✓	✗	<b>0.93</b>	<b>0.94</b>	<b>0.95</b>	<b>0.92</b>
	✓	✓	✓	<b>0.94</b>	<b>0.95</b>	<b>0.95</b>	<b>0.93</b>
MOTS-KITTI	✗	✗	✗	0.82	0.85	0.84	0.79
	✗	✓	✗	0.83	0.84	0.85	0.80
	✗	✓	✓	0.84	0.87	0.85	0.81
	✓	✓	✗	<b>0.90</b>	<b>0.90</b>	<b>0.87</b>	<b>0.83</b>
	✓	✓	✓	<b>0.90</b>	<b>0.91</b>	<b>0.88</b>	<b>0.83</b>

4%, 5%, and 8% for Sprites, DAVIS, MOT17, and KITTI datasets respectively when we use all the components of Alg. 1.

## 6 Conclusions

The proposed DHAE learns the contribution of shape and location features from multi-object video datasets by learning task-dependent uncertainties and improves the clustering performance by using constraints from sequential data patterns. Our experimental results show that our method can accurately cluster multiple objects using the embeddings from the DHAE. This method can be extended without significant modifications to include additional tasks of interest in similar scenarios such as object appearance and motion patterns. In the future, we intend to extend our method with target motion models and more robust birth/death/occlusion detection techniques so that it can be employed as a data association mechanism to the problems of multiple object tracking [41] and video instance segmentation [42].

## References

1. Elhamifar, E., Vidal, R.: Sparse subspace clustering: Algorithm, theory, and applications. *IEEE transactions on pattern analysis and machine intelligence* **35** (2013)

2765–2781 1, 3

2. Kulshreshtha, P., Guha, T.: An online algorithm for constrained face clustering in videos. In: ICIP. (2018) 2670–2674 1, 3
3. Tapaswi, M., Law, M.T., Fidler, S.: Video face clustering with unknown number of clusters. In: ICCV. (2019) 1, 3
4. Finn, C., Tan, X.Y., Duan, Y., Darrell, T., Levine, S., Abbeel, P.: Deep spatial autoencoders for visuomotor learning. In: ICRA. (2016) 512–519 1
5. Guo, Y., Gao, J., Li, F.: Spatial subspace clustering for drill hope spectral data. *Journal of Applied Remote Sensing* **8** (2014) 083644 1
6. Ji, P., Zhang, T., Li, H., Salzmann, M., Reid, I.: Deep subspace clustering networks. In: NIPS. NIPS'17, USA, Curran Associates Inc. (2017) 23–32 1, 3, 4
7. Xie, J., Girshick, R., Farhadi, A.: Unsupervised deep embedding for clustering analysis. In Balcan, M.F., Weinberger, K.Q., eds.: ICML. Volume 48 of PMLR., New York, New York, USA, PMLR (2016) 478–487 1, 3, 11
8. Zhou, P., Hou, Y., Feng, J.: Deep adversarial subspace clustering. In: CVPR. (2018) 1596–1604 1, 3, 11
9. Caron, M., Bojanowski, P., Joulin, A., Douze, M.: Deep clustering for unsupervised learning of visual features. *CoRR* **abs/1807.05520** (2018) 1, 3
10. Payer, C., Stern, D., Neff, T., Bischof, H., Urschler, M.: Instance segmentation and tracking with cosine embeddings and recurrent hourglass networks. *CoRR* **abs/1806.02070** (2018) 1
11. Ngiam, J., Khosla, A., Kim, M., Nam, J., Lee, H., Ng, A.Y.: Multimodal deep learning. In: ICML. ICML'11, USA, Omnipress (2011) 689–696 2
12. Cipolla, R., Gal, Y., Kendall, A.: Multi-task learning using uncertainty to weigh losses for scene geometry and semantics. In: CVPR. (2018) 7482–7491 2, 3, 4, 5
13. Vidal, R.: Subspace clustering. *IEEE Signal Processing Magazine* **28** (2011) 52–68 3
14. Buml, M., Tapaswi, M., Stiefelhagen, R.: Semi-supervised learning with constraints for person identification in multimedia data. In: CVPR. (2013) 3602–3609 3
15. J.Rousseeuw, P.: Silhouettes: A graphical aid to the interpretation and validation of cluster analysis. In: Computational and Applied Mathematics. Volume 20., Society for Industrial and Applied Mathematics (1987) 5365 3
16. Schlkopf, B., Platt, J., Hofmann, T.: In: Efficient Learning of Sparse Representations with an Energy-Based Model. MITP (2007) 3
17. Cheng, Y.: Mean shift, mode seeking, and clustering. *IEEE Transactions on Pattern Analysis and Machine Intelligence* **17** (1995) 790–799 3
18. Liu, G., Lin, Z., Yu, Y.: Robust subspace segmentation by low-rank representation. In: ICML. ICML'10, USA, Omnipress (2010) 663–670 3
19. Mukherjee, S., Asnani, H., Lin, E., Kannan, S.: Clustergan : Latent space clustering in generative adversarial networks. *CoRR* **abs/1809.03627** (2018) 3, 11
20. Reznichenko, Y., Prampolini, E., Siddique, A., Medeiros, H., Odene, F.: Visual tracking with autoencoder-based maximum a posteriori data fusion. In: 2019 IEEE 43rd Annual Computer Software and Applications Conference (COMPSAC). Volume 1. (2019) 501–506 3
21. Tierney, S., Gao, J., Guo, Y.: Subspace clustering for sequential data. In: CVPR. (2014) 1019–1026 3, 12
22. Jalil Mozhdehi, R., Reznichenko, Y., Siddique, A., Medeiros, H.: Deep convolutional particle filter with adaptive correlation maps for visual tracking. In: ICIP. (2018) 3
23. Mozhdehi, R.J., Reznichenko, Y., Siddique, A., Medeiros, H.: Convolutional adaptive particle filter with multiple models for visual tracking. In: ISVC. (2018) 3

24. Jalil Mozhdehi, R., Medeiros, H.: Deep convolutional likelihood particle filter for visual tracking. In: IPCV. (2020) [3](#)
25. Cheng, B., Liu, G., Wang, J., Huang, Z., Yan, S.: Multi-task low-rank affinity pursuit for image segmentation. In: ICCV. (2011) 2439–2446 [3](#), [4](#), [5](#)
26. Wagstaff, K., Cardie, C., Rogers, S., Schrdl, S.: Constrained K-means clustering with background knowledge. In Brodley, C.E., Danyluk, A.P., eds.: International Conference on Machine Learning. (2001) 577–584 [3](#), [8](#)
27. Zamir, A.R., Dehghan, A., Shah, M.: Gmcpr-tracker: Global multi-object tracking using generalized minimum clique graphs. In: ECCV. (2012) [3](#)
28. He, K., Gkioxari, G., Dollr, P., Girshick, R.: Mask R-CNN. In: ICCV. (2017) 2980–2988 [4](#), [10](#), [12](#), [13](#)
29. Kim, B., Ye, J.C.: Mumford–Shah loss functional for image segmentation with deep learning. IEEE Transactions on Image Processing **29** (2019) 1856–1866 [4](#)
30. Dumoulin, V., Visin, F.: A guide to convolution arithmetic for deep learning. Stat **1050** (2018) 11 [6](#)
31. Zeiler, M.D.: Adadelta: an adaptive learning rate method. arXiv preprint arXiv:1212.5701 (2012) [6](#)
32. Arthur, D., Vassilvitskii, S.: k-means++: The advantages of careful seeding. In: Proceedings of the eighteenth annual ACM-SIAM symposium on Discrete algorithms, Society for Industrial and Applied Mathematics (2007) 1027–1035 [9](#)
33. He, Z., Li, J., Liu, D., He, H., Barber, D.: Tracking by animation: Unsupervised learning of multi-object attentive trackers. In: CVPR. (2019) [9](#), [10](#), [12](#)
34. Voigtlaender, P., Krause, M., Osep, A., Luiten, J., Sekar, B.B.G., Geiger, A., Leibe, B.: Mots: Multi-object tracking and segmentation. In: CVPR. (2019) [9](#)
35. Perazzi, F., Pont-Tuset, J., McWilliams, B., Gool, L.V., Gross, M., Sorkine-Hornung, A.: A benchmark dataset and evaluation methodology for video object segmentation. In: CVPR. (2016) 724–732 [9](#), [10](#)
36. Milan, A., Leal-Taixé, L., Reid, I.D., Roth, S., Schindler, K.: MOT16: A benchmark for multi-object tracking. CoRR **abs/1603.00831** (2016) [10](#), [12](#)
37. Geiger, A.: Are we ready for autonomous driving? the kitti vision benchmark suite. In: CVPR. CVPR '12, Washington, DC, USA, IEEE Computer Society (2012) 3354–3361 [10](#)
38. Strehl, A., Ghosh, J.: Cluster ensembles — a knowledge reuse framework for combining multiple partitions. J. Mach. Learn. Res. **3** (2003) 583–617 [11](#)
39. Hubert, L., Arabie, P.: Comparing partitions. Journal of Classification **2** (1985) 193–218 [11](#)
40. Stiefelhagen, R., Bernardin, K., Bowers, R., Garofolo, J., Mostefa, D., Soundararajan, P.: The CLEAR 2006 evaluation. In: CLEAR, Berlin, Heidelberg, Springer-Verlag (2007) 1–44 [11](#), [12](#)
41. Sun, S., Akhtar, N., Song, H., Mian, A.S., Shah, M.: Deep affinity network for multiple object tracking. IEEE transactions on pattern analysis and machine intelligence (2019) [14](#)
42. Luiten, J., Torr, P., Leibe, B.: Video instance segmentation 2019: A winning approach for combined detection, segmentation, classification and tracking. In: Proceedings of the IEEE International Conference on Computer Vision Workshops. (2019) 0–0 [14](#)